TECHNICAL ARTICLE

Measurement and Simulation of Vacancy Formation in 2-MeV Self-irradiated Pure Fe

R. AUGUSTE,[1,6] M.O. LIEDKE,[2] F.A. SELIM,[3] B.P. UBERUAGA,[4] A. WAGNER,[2] and P. HOSEMANN[1,5]

1.—Department of Nuclear Engineering, University of California, Berkeley, CA, USA. 2.—Institute of Radiation Physics, Helmholtz-Zentrum Dresden-Rossendorf, Bautzner Landstr. 400, 01328 Dresden, Germany. 3.—Department of Physics and Astronomy, Bowling Green State University, Bowling Green, OH 43403, USA. 4.—Materials Science and Technology Division, Los Alamos National Laboratory, Los Alamos, NM 87545, USA. 5.—Material Science Division, Lawrence Berkeley National Laboratory, Berkeley, CA 94720, USA. 6.—e-mail: auguste@berkeley.edu

Positron annihilation spectroscopy is a powerful tool to quantify the amount of vacancies and vacancy clusters in materials. The technique has been utilized to study the induced defects in materials after ion beam and neutron irradiations. This paper makes the case for how the technique can and should be utilized to quantify the defects created by irradiation in situ during irradiation to foster a more thorough understanding of the surviving defects after initial collision cascades. This paper outlines a future experimental approach and its meaning for the nuclear materials community, being able to benchmark commonly used rate theory models of damage evolution.

INTRODUCTION

Radiation damage in materials is a fundamental problem faced by most nuclear technologies, e.g., fission, fusion, or accelerator-based techniques. Fundamentally, an incoming particle transfers a fraction (dependent of the masses) of its energy to a host lattice or induces a nuclear reaction. Further displacement damage in the material is caused by displacement cascades induced by either direct elastic collisions or inelastic events. This initial damage is what is usually characterized in the unit displacement per atom (dpa). While it is important to understand the amount of initial displacements produced, it is the evolution of these defects that causes the permanent property change, e.g., swelling, hardening, embrittlement, etc. The evolution as a function of temperature can be described using a rate theory approach. However, since this is a dynamic problem, experimental verification of either the displacement damage or its evolution has proven to be difficult. The studies featuring the quantification of the initial displacement damage are mostly indirect, including differential dilatometry,[1] electrical resistivity measurements,[2] or short intense ion beam pulses.[3]

Standard Rate Theory for Radiation Damage

The fundamental property of radiation damage is the creation of Frenkel pairs, so understanding the formation and evolution of monovacancies and interstitials is likewise fundamental to understanding radiation damage. The theory behind vacancy production from irradiation at different temperatures has been investigated previously, and the full equation for monovacancy concentration, C_{1v}, is given in Eq. 1[4]

$$
\begin{aligned}
C_{1v} &= C_{1v}^{\text{th}} + C_{1v}^{\text{ne}} \\
&= C_{1v}^{\text{th}} + \frac{1}{2}C\left\{\left(1 + 4 \times \frac{\dot{n}v_ip_i}{Av_vp_v}\frac{1}{C^2}\right)^{\frac{1}{2}} - 1\right\} \\
&\text{with}\quad C = \frac{v_ip_i}{A} + C_{1v}^{\text{th}} + \frac{C_{1v}^{\text{th}}v_ip_i}{v_vp_v}\quad \text{and} \\
A &= v_ia_i + v_va_v
\end{aligned}
\tag{1}
$$

where $\dot{n}$ represents the displacements per atom per second (dpa/s, dpa rate), p_i is the sink annihilation probability for interstitials, p_v is the sink annihilation probability for vacancies, v_i is the frequency factor for interstitials, v_v is the frequency factor for vacancies, a_i is the recombination factor for interstitials, and a_v is the recombination factor for

vacancies. C_{1v}^{th} is the contribution of thermal mono-vacancies, and C_{1v}^{ne} is the contribution of nonequilibrium monovacancies from radiation damage. The point defects, interstitials, and vacancies are assumed to be produced randomly throughout the solid. They move by random walk through the lattice until they cease to exist either by recombination with the opposite type of defect or by incorporation into the lattice at fixed unsaturable sinks such as dislocations, grain boundaries, and voids. No attempt is made to treat the nucleation of vacancy clusters, voids, and interstitial loops quantitatively, but the basic theory can be extended to derive void growth rates or swelling rates from the total sink annihilation rates and the relative concentrations of sinks with preferential interstitial or vacancy absorption.[4]

At low temperatures, where C_{1v}^{th} is negligible, C_{1v} is dependent on the level of defect production (dpa rate), $\dot{n}$, from irradiation and the vacancy annihilation probability from the presence of sinks (p_v). As illustrated in Fig. 1, with increasing temperature, C_{1v} initially decreases, goes through a minimum, and then becomes indistinguishable from the
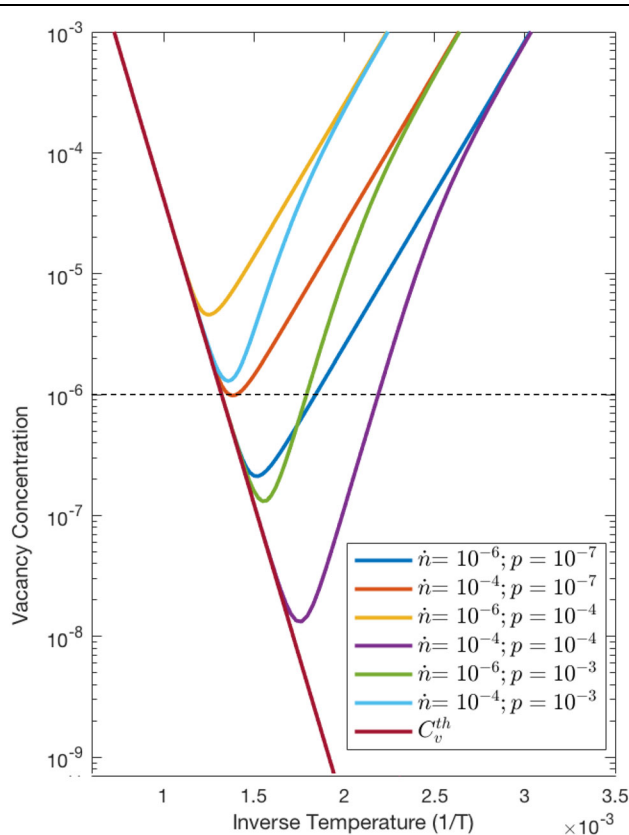

Fig. 1. Expected concentration of vacancies in Cu plotted as a function of inverse temperature, dpa rate ($\dot{n}$), and annihilation probability (p) according to Eq. 1 and Cu parameters from Wiedersich et al.[4] The low-temperature region limits thermal monovacancy formation, while at high temperature the vacancy concentration is dominated by the equilibrium vacancy concentration.

thermally produced vacancy concentration without defect production from radiation. In the low-temperature region, there is a small contribution from thermally produced vacancies, C_{1v}^{th}, while vacancies produced via radiation become more mobile with increasing temperature, increasing the likelihood of annihilation and decreasing C_{1v}. Ideally, nonequilibrium experiments should be done in this low-temperature region to measure the dominant effect of C_{1v}^{ne}. According to theory, increasing the dpa rate at low temperatures yields increasing concentration of vacancies, which can lead to larger extended defects such as large voids or vacancy clusters.

Larger extended defects in materials created by ion irradiation present a multiscale problem with defect lifetimes ranging from picoseconds to years.[5–7] There are a large number of transient displacements in the radiation cascade, but most self-anneal with a time scale on the order of picoseconds, leaving just a relatively small number of defects. These remaining defects are still nonequilibrium,[8] so capturing small point defects with short time scales must be done in situ, before further self-annealing and relaxation to larger, extended, more stable defects. Again, direct quantification and verification of Eq. 1 has not been conducted, since quantifying monovacancies during irradiation is not trivial.

Positron Implantation Theory

Positrons are a well-known nondestructive analytical probe for quantifying point defects and dislocations in materials. Positrons enter a solid, annihilate with electrons, and are further sensitive to local electron density within individual defects. Defects the size of voids down to monovacancies are regions with reduced electron density, resulting in less positron interaction. As such, positrons can be used to probe point defects at scales not visible in transmission electron microscopy (TEM) studies.[9–11] Positron annihilation spectroscopy (PAS) is a technique that uses the positron interaction with local electron density to estimate vacancy concentration within materials. PAS has previously been used to study radiation damage in steels and other nuclear materials, but most studies are ex situ after neutron or ion beam irradiation.[12–17] Previous PAS studies on reactor pressure vessel (RPV) steels showed the utility of the PAS technique to probe extended defects in previously irradiated steels.[18,19] In contrast, the present work combines simulated in situ radiation damage and PAS measurement to investigate the mechanism for monovacancy formation. Displacements formed during the ion beam irradiation damage cascade are expected to relax and agglomerate into larger surviving vacancy clusters that can be easily observed by PAS.

The theory behind positron stopping is well studied. When a positron penetrates into a solid, it loses its kinetic energy by ionization, excitation of

electrons, and scattering at phonons until its energy decreases down to the thermal energy $3/2\ k_\mathrm{b}T$, i.e., ~ 0.04 eV at room temperature.[20] This process is called thermalization and, in metallic materials, takes only a few picoseconds.[20] The positron implantation profile is described by the exponential probability density function, $P(z)$, in Eq. 2[20]

$$P(z) = \frac{1}{\bar{x}}e^{-\frac{z}{\bar{x}}},\qquad (2)$$

where z is the depth from the sample surface. The mean penetration depth of positrons, $\bar{x}$, is obtained by the Makhov positron stopping expression as a function of positron implantation energy, E, and using Eq. 3[20]

$$\bar{x} = \frac{A}{\rho}E^n,\qquad (3)$$

where $A = 3.6\ \mu\mathrm{g/cm^2\ keV^{-1.6}}$ and $n = 1.6$ are independent empirical parameters,[21] and ρ is the material density, which here is considered to be 7.874 g/cm^{-3} for pure iron. This stopping profile does not assume subsequent diffusion of positrons or formation of positronium.

In practice, positron spectroscopy on materials uses two main techniques, viz. positron annihilation lifetime spectroscopy (PALS) and Doppler broadening of the annihilation photopeak (DBS). PALS is based on the measurement of the time difference between the generation of a positron entering a medium and the γ rays from positron–electron annihilation. These time differences correspond to the lifetimes of individual positrons. By measuring the lifetimes of the positrons, one can obtain the electron density in the sample "seen" by positrons. Thus, the positron lifetime can be correlated with the electron density and ultimately with the size and density of vacancy-type defects within the sample. DBS is based on detection of the 511-keV characteristic annihilation γ-rays. The Doppler shift is measured by the broadening of the 511-keV peak in annihilation γ-rays resulting from the same annihilation event with an electron. The broadening of this peak from electron annihilation represents the electron momentum distribution seen by positrons and is very sensitive to the presence of vacancies, as positrons trapped in vacancies mainly annihilate with the low-momentum valence electrons leading to less broadening.

For DBS, the S-parameter indicates the relative contribution in the 511 keV peak from valence and conduction electrons, while the W-parameter represents the relative contribution from core electrons. The S and W parameters are calculated from the shape of the 511-keV peak as follows: S is calculated by dividing the counts in the central region of the peak into total counts in the peak, while W is calculated by dividing the counts in the two wings of the peak into the total counts in the peak, as illustrated in Fig. 2. S is higher for positrons
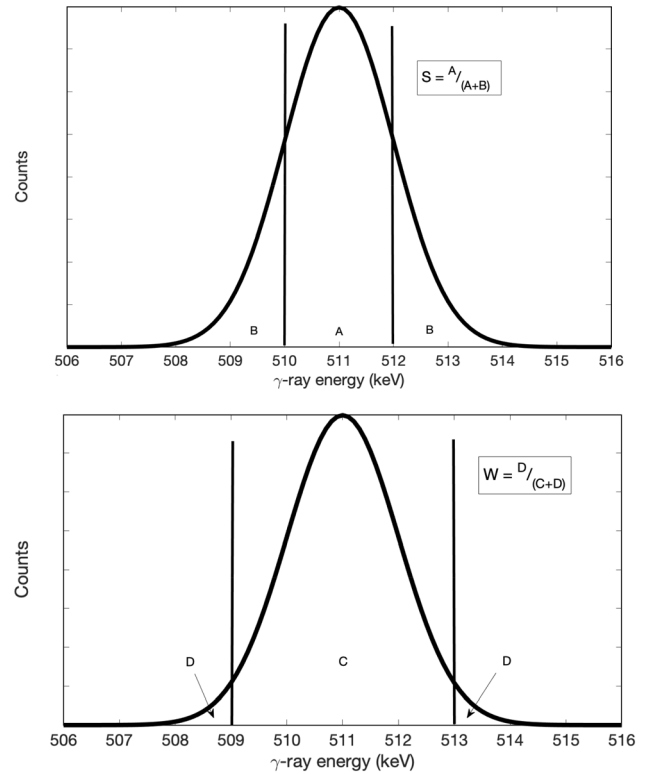

Fig. 2. DBS calculation of S and W parameters from detection of 511-keV characteristic annihilation γ-rays.

trapped at and annihilated in open-volume defects. Positron lifetime spectroscopy enables identification of defects in solids and determines their concentrations, while Doppler broadening mainly provides information on the overall defect concentration, and coincident Doppler broadening can provide information about the local chemical environment of defects.[22,23]

Recently, ex situ studies have appeared regarding radiation damage using TEM, atom probe tomography, PALS, and DBS techniques on Fe–Cr alloys[24] and RPV steels.[18,19] In both cases, defect mobility was driven by dose rate and temperature, leading to irradiation hardening at higher observed doses. The studies suggest point defects and vacancy cluster defects induce the formation of dislocation loops, but are not able to quantify the effect from vacancy-type defects without in situ PAS observation. To fill this gap, the present study aims to compare defect measurements using just PALS and DBS techniques to the theory behind radiation-produced monovacancies.

This work, however, features the importance and feasibility of directly combining in situ PALS with ion-beam irradiation to investigate monovacancy formation theory. The objective of this paper is to provide the theoretical and computational background necessary for the in situ technique. Currently, there are limited experimental facilities to perform these in situ measurements, but this work is a first attempt to capture such experiments

theoretically and benchmark the theoretical considerations with ex situ PAS experiments. Previous in situ experiments have been limited to just Doppler broadening PAS[25,26] using low-energy slow positrons with low penetration depth.[27,28] A schematic of a future experimental setup, using high-energy positrons and lifetime spectroscopy during ion irradiation, is shown in Fig. 3. In the future, such in situ experiments must be carried out to verify and refine the rate theory approach mentioned above. Moreover, in situ experiments are needed to understand the true defect content of materials during irradiation, as that will drive the materials' response in a number of contexts, including irradiation environments with added corrosion, pressure, or stress. Ex situ experiments cannot provide the same level of understanding because of the small size, high mobility, and inherent instability of defects outside the radiation damage cascade.

METHODS

Overview of Methods

To analyze monovacancies and extended defects in ion-irradiated Fe, a hypothetical in situ experiment simulates ion beam irradiation with coincident simultaneous positron lifetime spectroscopy on a pure Fe sample. An overview of the methods used in this paper is depicted in Fig. 4, explaining the parallels between the simulation in this paper and future experimental approaches. This paper is meant to provide a computational model using theoretical positron stopping and radiation damage theory for a future in situ experiment.

Radiation Damage and Positron Stopping Profile

As a proof of principle, a positron implantation profile should overlap the expected damage region from the ion beam. Using the resulting damage cascade profile from Stopping and Range of Ions in Matter (SRIM) ("Positron Implantation Modeling" section), the positron implantation profile for 16 keV was overlaid to calculate the sampling depth of the positrons. At 16 keV, the positrons sampled most of the damage across the dpa profile, especially in the 0 nm to 500 nm region, as shown in Fig. 5.

Furthermore, it is ideal for the positrons to implant and sample locally within the maximum damage region from the ion beam. To do this, the incoming positron beam must be energetically narrow relative to the ion beam full-width at half-maximum (FWHM) so all incoming positrons sample the near-constant dpa region. Figure 6 shows a three-dimensional (3D) representation of the overlap between the incoming beam. Ion and positron beam percentages are shown at different x–y positions in the sample, that is, what percent of particles from the overall beams will be present at each location. The positron beam FWHM is less than the ion beam FWHM, so positrons will primarily locally sample the damage region from the ions.

Overview of Modeling

The model simulation of in situ ion beam irradiation and positron annihilation spectroscopy performed here uses a voxel approach in MATLAB software[29] to simulate the radiation damage from the ion beam and coincident positron implantation from the positron beam. The sample is modeled as if it were split into geometric cubes, called voxels, and local information about ion beam and positron beam effects for each voxel is stored as a 3D matrix in MATLAB.[29] Ion beam damage and positron implantation rates are stored in these 3D voxel matrices for
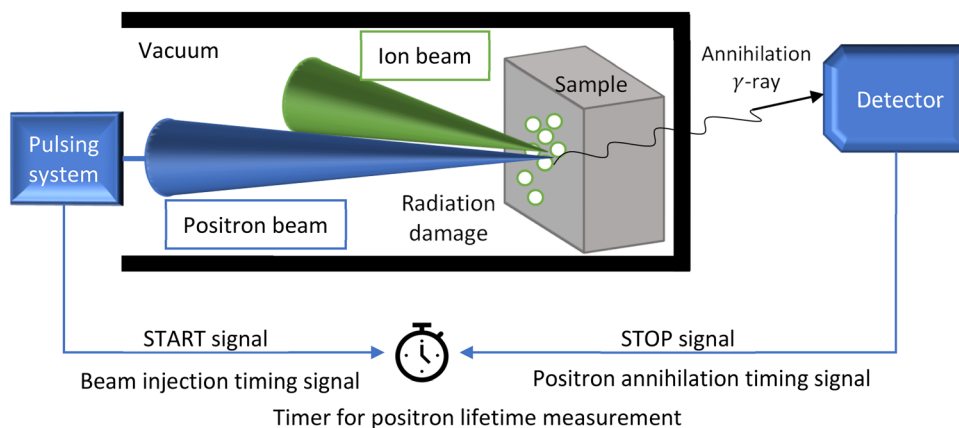

Fig. 3. Schematic of coincident ion beam and pulsed positron beam for in situ PAS experiments during radiation damage. Pulsed positrons measure defect concentration during ion irradiation by entering sample, annihilating with electrons, and detecting timing of resulting annihilation γ-rays.
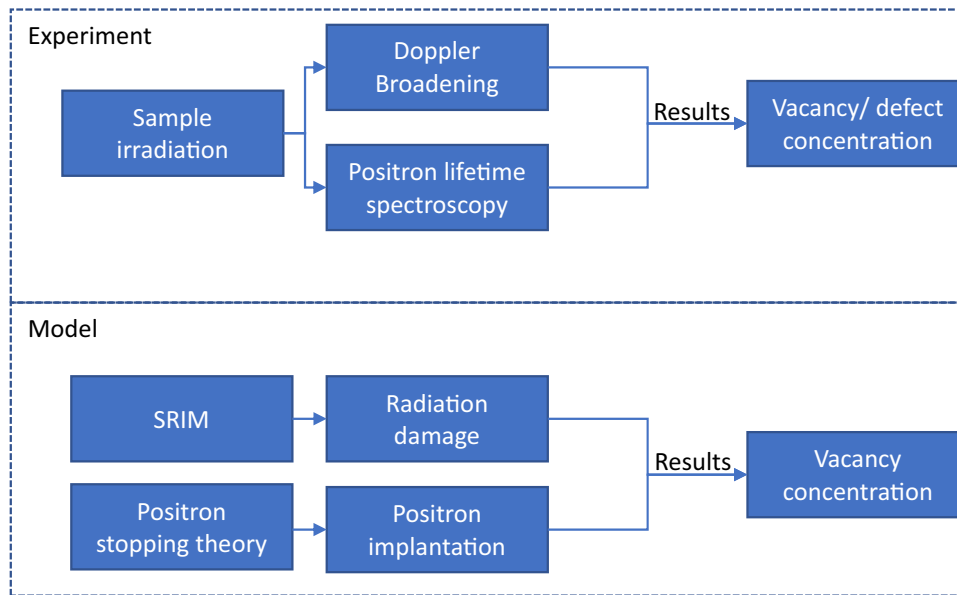
Fig. 4. Overview of methods from hypothetical experiment and modeling efforts. Experimental effort would involve in situ positron spectroscopy (DBS and PALS) on small radiation-induced defects. Conversely, modeling of an in situ simultaneous irradiation and PALS experiment on vacancy concentration was carried out using radiation damage and positron stopping theory.
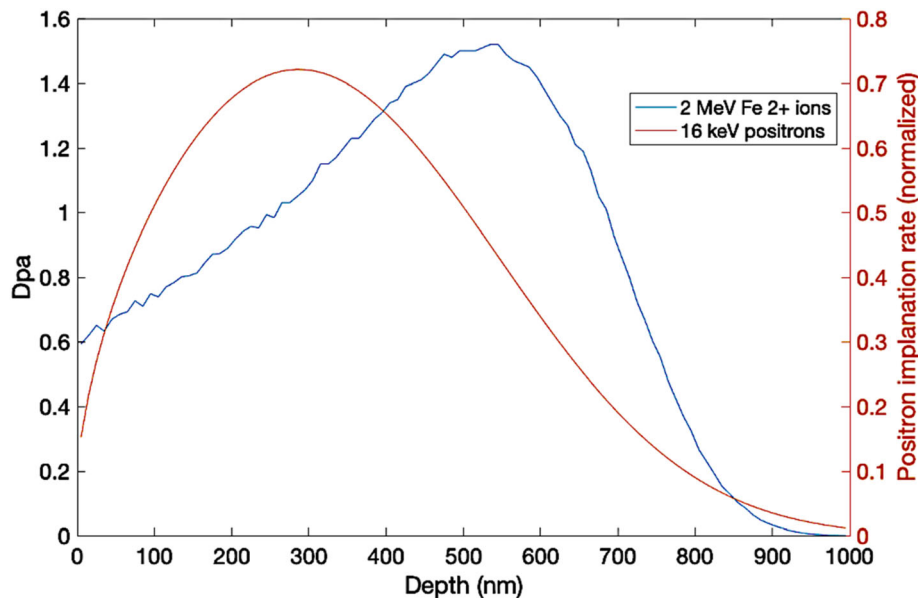

Fig. 5. Overlap of damage profile in Fe (dpa shown in units of vacancies per angstrom-ion) when irradiated with 2-MeV Fe^{2+} ions, as simulated by SRIM, and Makhovian implantation profile of positrons at energies of 16 keV (Eq. 2). Positrons implanted at 16 keV, not accounting for subsequent diffusion, show a significant overlap with radiation profile from 0 nm to 500 nm than when implanted at lower energies, providing a depth-dependent interaction with damage.

locations inside the sample, and two matrices—(1) vacancy concentration from ion radiation damage and (2) positron implantation rate from coincident positron beam—are overlaid to calculate how many in situ monovacancies in a single voxel are "seen" by incoming positrons. Performing these simulations will help compare theoretical results of the present study with future experimental efforts combining ion beam irradiation and simultaneous positron annihilation spectroscopy.

Radiation Damage Cascade Modeling

Radiation damage in Fe was simulated using the parameters of the ion beam at Los Alamos National Laboratory (LANL) ("Radiation Damage and Positron Stopping Profile" section) and standard radiation damage rate theory (Eq. 1). SRIM-2008[30] was used to determine the vacancy formation rate from the ion beam. In the SRIM simulations, a displacement threshold energy of 40 eV was assumed for
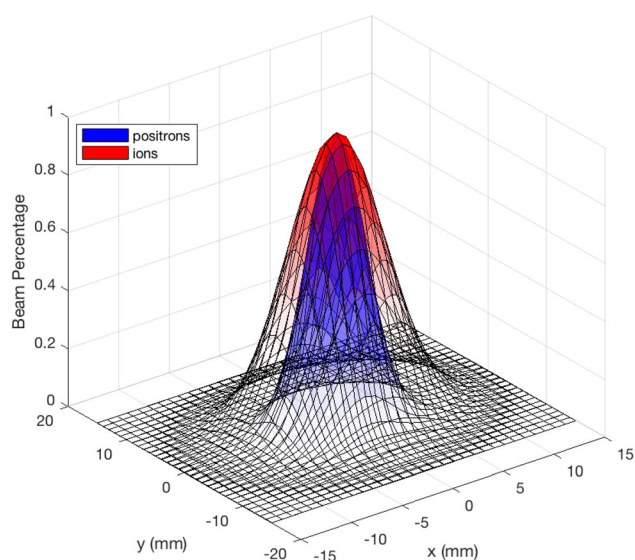
Fig. 6. 3D representation of overlap between beam intensities from ion irradiation and positron implantation. Normalized beam percentages shown for comparison, or what percent of particles from each incoming beam is present at different x–y locations in sample. Ideally, positron beam intensity profile should be narrow and fit inside the ion beam for positrons to sample locally within maximum damage region left by ion beam.

Fe,[31] and the Fe density was 7.874 g/cm^3. These simulations were run in the full cascade mode. At this point, it is important to note that a full cascade delivers about a factor of two higher dose rate as the quick Kinchin–Pease (K–P) model. The quick K–P model only follows the primary knock-on atom path through the material, but the detailed model considers all the secondary knock-on atoms causing chains of further displacements within the material. Further, the quick K–P model is the same model used in MCNP calculations and is highlighted in the ASTM standard by Stoller et al.[31,32] For the purpose of this discussion, here one may use the calculation as a guideline and divide the dose rate caused by the incoming ion beam by a factor of two for the quick K–P model. In either case, incident positrons will sample only a fraction of total damage delivered ($\sim 10^{-3}$ defects sampled), so the differences between detailed cascade and quick K–P model do not change the feasibility of this proposed experiment. To truly compare the measured defects as a function of dose rate with the calculated nonequilibrium surviving defects, one would absolutely have to use detailed modeling calculations [e.g., molecular dynamics (MD)].

The model characterizes the ion beam intensity (in μA/mm^2) using a Gaussian beam profile and beam FWHM of 10 mm for incident 2-MeV Fe^{2+} ions into pure Fe at room temperature (293.15 K). The ion beam intensity is assumed to be the symmetric in the x–y directions, perpendicular to the ion beam propagation into the sample (z), and the sample is irradiated to a total fluence of 5.65×10^{14} ions/cm^2.

Combining vacancy calculations from SRIM-2008 and the ion beam intensity from the LANL beam parameters, the model then calculates the dpa rate (in dpa/s) in the Fe sample at different locations inside the sample. The expected vacancy concentration is calculated from the standard rate theory calculation (Eq. 1) using the dpa rate within the sample. The expected vacancy concentration is stored as a 3D matrix measuring radiation damage at each position inside the sample. This radiation damage cascade matrix was then overlaid with the positron implantation rate matrix to calculate a 3D matrix with the observable monovacancy concentration "seen" by the positrons, giving the PAS-observable monovacancy concentration at each location inside the sample.

Positron Implantation Modeling

The positron implantation rate was simulated using the parameters of the positron beam at the Helmholtz-Zentrum Dresden-Rossendorf (HZDR) in Dresden, Germany ("Overview of Modelling" section)[26] and a Mahkov positron implantation profile from literature (Eqs. 2 and 3).[20] The positron beam intensity (in positrons/s mm^2) is calculated from a Gaussian beam profile with FWHM of 6 mm for a fluence of 10^6 positrons/s. Similar to the ion beam, the positron beam intensity is symmetric in the x–y directions, perpendicular to the beam propagation (z).

The positron implantation rate is the probability of a positron being at a particular voxel or thermalizing at a particular location inside the sample (Eq. 3), and thus being available to interact with a vacancy within a voxel. Again, we neglect subsequent migration of the positrons in this analysis. The implantation rate normalized the number of positrons found at a particular location within a voxel to the total number of positrons in the incoming beam. Finally, the 3D radiation damage cascade matrix was overlaid with the positron implantation rate 3D matrix to calculate a 3D matrix of the PAS-observable monovacancy concentration at each location inside the sample. This calculation assumes both beam centers are concentric and aligned normal to the sample surface. The average PAS-observable vacancy concentration over the entire 3D matrix for each location in the sample is shown in the results.

RESULTS

Modeling Results

The damage profile from SRIM was used to calculate a dpa-dependent vacancy concentration using Eq. 1, and Fig. 7 shows the vacancy concentration in four different planes, or slices, of the implanted Fe. The increase in vacancy concentration trend between 0 nm and 400 nm seen in the damage profile in Fig. 5 can also be observed.
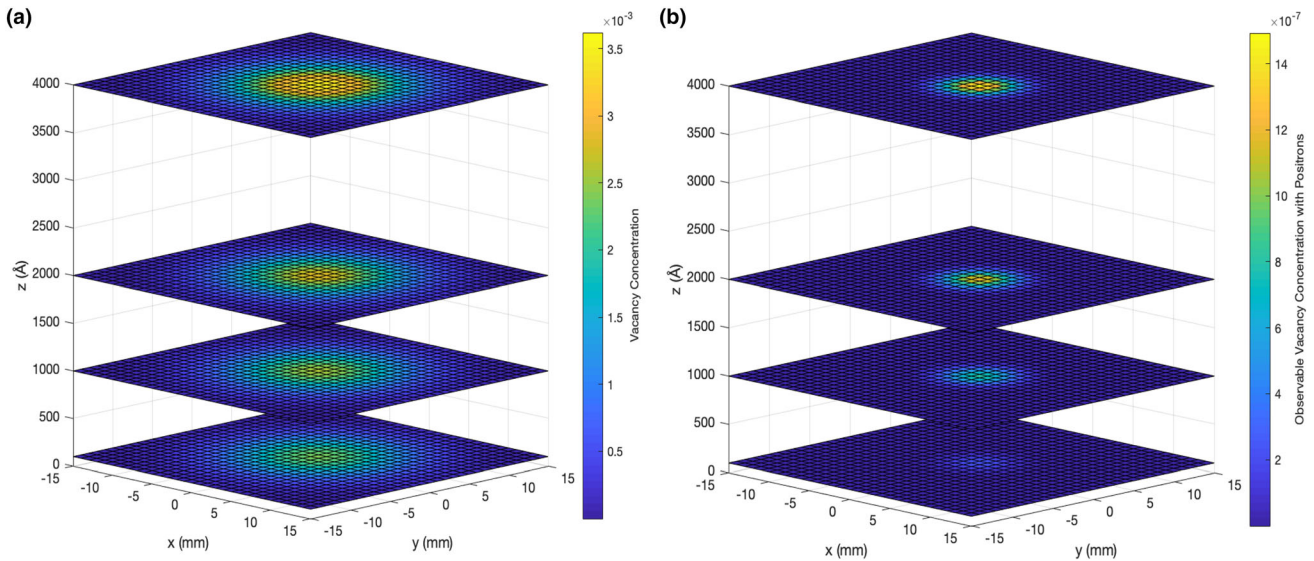
(a)

(b)

Fig. 7. (a) Calculated vacancy concentration due to radiation damage cascade in situ by 2-MeV Fe^{2+} ions into Fe. Slices taken at 10 nm, 100 nm, 200 nm, and 400 nm. Ion beam incoming from [centered at (0,0,0)]. Damage increases as depth increases along the center line of the sample, as expected in SRIM calculations; (b) Simulated vacancy concentration after overlapping positron implantation profile from 16 keV positrons. Slices again taken at 10 nm, 100 nm, 200 nm, and 400 nm. Damage still increases as depth increases along the center line of the sample, but fewer vacancies are observed by positrons than actually calculated by SRIM, shown in (a).

Finally, overlaying the expected vacancy concentration and positron implantation profile (Fig. 7b) yields the observed vacancy concentration from monovacancy-sampling positrons, the expected results of an in situ experiment accounting for the sampling efficiency and positron vacancy interaction as outlined above. The positron implantation profile used in Fig. 7b was for 16-keV positrons (Fig. 5). The decrease in observed vacancy concentration (Fig. 7b) versus the calculated vacancy concentration (Fig. 7a) is due to the fact that not all monovacancies will be sampled by incoming positrons. The model used does not include diffusion of positrons after implantation, and positrons may in fact sample more vacancies during diffusion than calculated here. However, the same trend of increasing vacancy concentration from 0 nm to 400 nm along the centerline can be seen.

The total observed vacancy concentration inside the sample is calculated by summing over vacancy concentration in all sample voxels. We ran the simulation for three cases, one with the ion beam off and the other two with the ion beam on at different beam currents. The observed vacancy concentration at different depths was calculated for each case by varying the incident positron energy from 2 keV to 16 keV. Increasing positron energy increases the mean implantation depth, sending more positrons to sample deeper into the material.[20] With the ion beam off, the observed concentration was small, 9.1×10^{-33}, and constant from 2 keV to 16 keV. Only thermal monovacancies at room temperature were present in the sample without the monovacancies from radiation damage. Turning on the ion
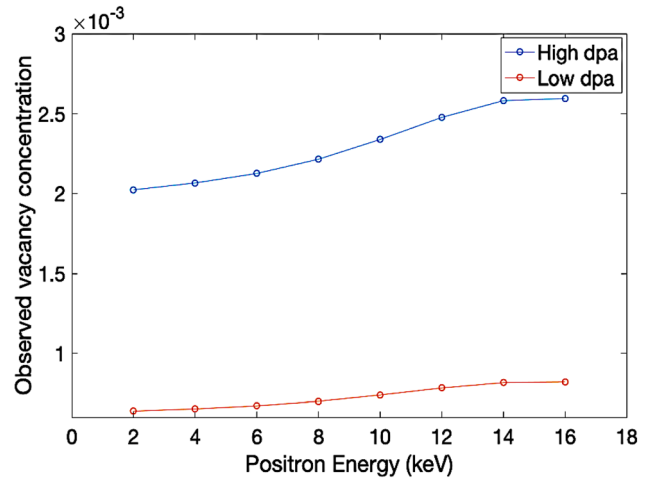

Fig. 8. Simulated positron-observable monovacancy concentration as a function of dose, obtained by varying incident sampling positron energy from 2 keV to 16 keV.

beam drastically increased the observed vacancy concentration inside the sample to a range of 10^{-4} to 10^{-3}. In agreement with rate theory,[4] at low temperatures, the effect of thermal vacancies was determined to be negligible.

Simulated vacancy concentrations as a function of incoming positron energy for the two cases with the ion beam on are plotted in Fig. 8. A trend of increasing vacancy concentration as a function of depth matches the SRIM damage cascade results in Fig. 5, which is in good agreement with the 2-MeV damage simulations. Simulating the same

experiment for a higher dpa case (an order of magnitude greater beam current) yields an increase in vacancy concentration, and the increase in vacancy concentration at higher depths inside the sample means the peak in the damage cascade around 500 nm becomes more pronounced. The vacancy concentration increases significantly when irradiated to 0.06 (high) dpa as compared with the defect concentration when the dose was decreased one order of magnitude to 0.006 (low) dpa. A future in situ experimental setup could cycle the ion beam off after some time and measure the decay of the radiation damage monovacancies.

There are limits to the positron implantation and damage cascade simulation techniques used here. Positrons diffuse back to the surface and can form positronium, relevant for positron energies below 2 keV.[33] Second, the damage cascade simulates dpa rate, but only the formation of monovacancies without other extended defects such as divacancies, large vacancy clusters, or dislocation loops. Extended defects seen in previous ex situ TEM results[18,34] after the damage cascade were not modeled in the PAS simulations here. Even in the simulated high-dpa case, the saturation limit of positron trapping may even be reached (about 1×10^{-3}), and in saturation positrons, only detect the defect type with highest positron trapping rate. Future investigations should focus on resolving different trapping sites with PAS.

Despite these limits, the in situ computational model in this work shows the effectiveness of PAS in capturing small vacancies associated with ion irradiation. The pulsed variable energy positron beam allows one to use positrons for in situ ion-irradiated samples, a new ability in providing quantitative description for their density even in the case of positron trapping at monovacancies. Monovacancies are among the smallest defects, too small to observe with TEM, but are the embryos for larger vacancy clusters, dislocation loops, and voids. Observing increases in monovacancy concentration from the damage cascade offers new insights on the fundamental evolution and growth of larger defects. Positron spectroscopy is a promising nondestructive tool for the investigation of the damage cascade in situ, and its effectiveness can be seen even when compared with ex situ PAS of larger defects after the end of the damage cascade.

The promise of the in situ technique for coincident ion irradiation and PAS is to directly observe the damage cascade in a way not previously possible. Experimental PAS techniques are able to observe the smallest vacancy clusters, but in situ PAS studies to investigate concentration of monovacancies during irradiation are underdeveloped. Studying the fundamental Frenkel pair creation for vacancies in radiation damage is highly important and was modeled in this work, but the full validation of standard rate theory cannot be entirely experimentally investigated without combining simultaneous PAS and ion irradiation in situ in a future study. Monovacancy creation during ion irradiation, survival rate after radiation, and agglomeration of vacancies to extended defects can be studied by further developing the PALS and DBS techniques demonstrated here.

CONCLUSION

This theory and simulation work show the effectiveness of PAS both in capturing small monovacancies associated with ion irradiation and in providing quantitative description for their size and density even in the case of saturated positron trapping at defects. Pulsed variable-energy positron beams allow for nondestructive investigation of radiation damage featuring small defects. Combining ion-irradiation and PAS techniques experimentally uniquely allows one to probe the size and distribution of small defects as a function of dose in situ.

Monovacancy concentration was shown in simulation to increase in situ with increasing dpa; however, surviving monovacancies ex situ may not directly be detected as Fe monovacancies are unstable and often highly mobile unless trapped at impurities. The promise of using PAS techniques for additional in situ studies for probing monovacancies and evolution of extended defects is demonstrated herein because monovacancies are too small for ex situ TEM studies and unstable outside of the radiation damage cascade. Investigating monovacancy evolution in situ is highly important because they are embryos for larger stable extended defects during and after irradiation such as vacancy clusters or voids.

ACKNOWLEDGEMENTS

REFERENCES

1. R. Kerl, J. Wolff, and T. Hehenkamp, *Intermetallics* 7, 301 (1999).
2. C. Dimitrov, M. Tenti, and O. Dimitrov, *J. Phys. F Met. Phys.* 11, 753 (1981).
3. A. Persaud, J.J. Barnard, H. Guo, P. Hosemann, S. Lidia, A.M. Minor, P.A. Seidl, and T. Schenkel, *Phys. Procedia* 66, 604 (2015).
4. H. Wiedersich, *Radiat. Eff.* 12, 111 (1972).
5. B.D. Wirth, M.J. Caturla, T. DíazDeLaRubia, T. Khraishi, and H. Zbib, *Nucl. Instrum. Methods Phys. Res. Sect. B* 180, 23 (2001).
6. J.S. Robach, I.M. Robertson, B.D. Wirth, and A. Arsenlis, *Philos. Mag.* 83, 955 (2003).
7. B.D. Wirth, X. Hu, A. Kohnert, and D.J. Xu, *J. Mater. Res.* 30, 1440 (2015).
8. E. Roger, *Stoller, Primary Radiation Damage Formation*, 1st ed. (Amsterdam: Elsevier, 2019), pp. 293–332.
9. C. Lu, K. Jin, L.K. Béland, F. Zhang, T. Yang, L. Qiao, Y. Zhang, H. Bei, H.M. Christen, R.E. Stoller, and L. Wang, *Sci. Rep.* 6, 19994 (2016).

10. X. Yi, M.L. Jenkins, K. Hattar, P.D. Edmondson, and S.G. Roberts, *Acta Mater.* 92, 163 (2015).
11. C. Liu, L. He, Y. Zhai, B. Tyburska-Püschel, P.M. Voyles, K. Sridharan, D. Morgan, and I. Szlufarska, *Acta Mater.* 125, 377 (2017).
12. Y. Nagai, K. Takadate, Z. Tang, H. Ohkubo, H. Sunaga, H. Takizawa, and M. Hasegawa, *Phys. Rev. B* 67, 224202 (2003).
13. T. Onitsuka, M. Takenaka, E. Kuramoto, Y. Nagai, and M. Hasegawa, *Phys. Rev. B* 65, 012204 (2001).
14. Y. Nagai, Z. Tang, M. Hassegawa, T. Kanai, and M. Saneyasu, *Phys. Rev. B* 63, 134110 (2001).
15. J. Čížek, F. Lukáč, I. Procházka, R. Kužel, Y. Jirásková, D. Janičkovič, W. Anwand, and G. Brauer, *Phys. B (Amsterdam, Neth.)* 407, 2659 (2012).
16. A. Vehanen, P. Hautojarvi, J. Johansson, J. Yli-Kauppila, and P. Moser, *Phys. Rev. B* 25, 762 (1982).
17. V. Krsjak, J. Kuriplach, T. Shen, V. Sabelova, K. Sato, and Y. Dai, *J. Nucl. Mater.* 456, 382 (2015).
18. J. Jiang, Y.C. Wu, X.B. Liu, R.S. Wang, Y. Nagai, K. Inoue, Y. Shimizu, and T. Toyama, *J. Nucl. Mater.* 458, 326 (2015).
19. X. Liu, R. Wang, A. Ren, P. Huang, Y. Wu, J. Jiang, C. Zhang, and X. Wang, *Radiat. Phys. Chem.* 81, 1586 (2012).
20. J. Čížek, I. Procházka, and J. Kocik, *Defect Diffus. Forum* 273, 81 (2008).
21. P. Hautojärvi, *Positrons in Solids*, 1st ed. (Berlin: Springer, 1979), pp. 491–522.
22. P. Kirkegaard, J. Olsen, and M. Eldrup, *PALSfit3: A Software Package for Analyzing Positron Lifetime Spectra* (Lyngby: Technical University of Denmark, 2017).
23. A. van Veen, H. Schut, J. de Vries, R.A. Hakvoort, and M.R. Ijpma, *AIP Conf. Proc.* 218–1, 171 (1991).
24. C.D. Hardie, C.A. Williams, S. Xu, and S.G. Roberts, *J. Nucl. Mater.* 439, 33 (2013).
25. M.O. Liedke, W. Anwand, R. Bali, S. Cornelius, M. Butterling, T.T. Trinh, A. Wagner, S. Salamon, D. Walecki, A. Smekhova, H. Wende, and K. Potzger, *J. Appl. Phys. (Melville, NY, USA)* 117, 163908 (2015).
26. A. Wagner, M. Butterling, M.O. Liedke, K. Potzger, and R. Krause-Rehberg, *AIP Conf. Proc.* 1, 040003 (2018).
27. A. Kinomura, R. Suzuki, T. Ohdaira, N. Oshima, B.E. O'Rourke, and T. Nishijima, *Phys. Procedia* 35, 111 (2012).
28. A. Kinomura, R. Suzuki, T. Ohdaira, N. Oshima, B.E. O'Rourke, and T. Nishijima, *J. Phys. Conf. Ser.* 443, 012043 (2013).
29. MATLAB. Version 9.4.0 R (2018a). Natick, MA: The MathWorks Inc., (2018).
30. J.F. Ziegler and J.P. Biersack. SRIM-2008, Stopping power and range of ions in matter (2008).
31. R.E. Stoller, M.B. Toloczko, G.S. Was, A.G. Certain, S. Dwaraknath, and F.A. Garner, *Nucl. Instrum. Methods Phys. Res. Sect. B* 310, 75 (2013).
32. ASTM Standards, *ASTM International*, PA, E706(ID), ASTM E693-12 (2012).
33. A. Seeger, *Appl. Surf. Sci.* 85, 8 (1995).
34. J. Shi, W.Z. Zhao, Y.C. Wu, X.B. Liu, and J. Jiang, *Nucl. Instrum. Methods Phys. Res. Sect. B* 443, 62 (2019).